Indian Journal of Chemistry
Vol. 60A, November 2021, pp. 1409-1415

Synthesis, crystal structure, luminescent, and photocatalytic properties of a uranyl(VI)-organic framework based on tripodal flexible zwitterionic ligand

Yuning Meng, Fei Niu, Xiaolin Zhang, Donghui Liu, Qiaofa Lan & Youming Yang*

Faculty of Materials, Metallurgy and Chemistry, Jiangxi University of Science and Technology, Ganzhou 341000, P R China

*E-mail: yanguming@126.com

Received 25 August 2021; revised and accepted 13 October 2021

The uranyl-organic framework based tripodal flexible zwitterion ligand 1,1',1"-[benzene-1,3,5-triyltris(methylene)] tris(pyridine-4-carboxylic acid) tribromine (H_3LBr_3), $[(UO_2)_2(\mu_3\text{-}O)(\mu_2\text{-}OH)L]NO_3{\cdot}nH_2O$ (n ≈ 5) (**1**) has been synthesized under hydrothermal condition and characterized by elemental analysis, IR spectroscopy, single-crystal X-ray diffraction, powder X-ray diffraction, thermogravimetric analysis, and UV-visible spectroscopy. Compound **1** contains a tetra-uranyl oxo-cluster, which displays a microporous 3D structure. The fluorescence measurement shows that **1** exhibits strong luminescence. Furthermore, **1** shows good photocatalytic activity for the degradation of methylene blue.

Keywords: Uranyl-organic framework, Flexible zwitterionic Ligand, Photoluminescent properties, Photocatalytic degradation, Methylene blue

Over the past two decades, more and more uranyl-organic frameworks (UOFs) have been studied[1-7]. Because the pore structure and pore size can be regulated by adjusting the ligands, UOFs demonstrate a variety of structures and topologies, and show great potential in many fields, such as photocatalysis[8-10], ion exchange[11,12], fluorescent probes[13-15], molecular adsorption of organic dyes[16-19], fluorescent materials[20,21], and so on.

Photocatalytic technology is an attractive method to resolve water pollution, especially through the potential to photocatalytically degrade organic substrates using uranyl complexes, with particular emphasis on UOFs[22-26]. There are many reports on the use of UOFs as photocatalysts for the degradation of organic dyes. For example, Zheng and co-workers have reported several UOFs as photocatalysts for the degradation of rhodamine B (RhB) under daylight irradiation with good results[27]. Xing and Bai synthesized two UOFs that were able to degrade RhB with the ligand 1,2,4,5-benzenetetracarboxylic acid[28]. Meanwhile, Chen synthesized three UOFs, one of which possessed Ag as a heteroatom. They were able to prove that the center of photocatalysis for degradation of RhB was the uranyl ion[29]. Bai reported three UOFs which contained Cu as the heteroatom, and at the same time investigated the degradation of methylene blue (MB)[30].

Usually, due to the polar positions are occupied by two double-bonded oxygen atoms, uranyl can only coordinate with oxygen, nitrogen or sulfur from the ligands in the axial direction to form tetragonal, pentagonal and hexagonal bipyramidal polyhedrons. To the best of our knowledge, 3D cationic UOFs are rare due to the two oxygen atoms of the uranyl positioned along the axis and the additional negative charge on the ligands. Wang previously reported two tetra-nuclear uranyl oxo-cluster UOFs based on 1,1′,1″-(2,4,6-trimethylbenzene-1,3,5-triyl)-tris(methylene)-tris(pyridine-4-carboxylic acid) tribromine($H_3L^*Br_3$), $[(UO_2)_2L^*(OH)O(COOH)]{\cdot}1.5$ $DMF{\cdot}7H_2O$(SCU-6, 2D UOF) and $[(UO_2)L^*(OH)]$ $Br{\cdot}1.5DMF{\cdot}4H_2O$ (SCU-7, 2D cationic UOF) via solvothermal reactions[31]. In addition, Zhao and co-workers reported two UOFs using $H_3L^*Cl_3$ in reactions with uranyl cations under hydrothermal conditions: $[(UO_2)_4L^*_2Cl_4(\mu_3\text{-}O)_2]{\cdot}4H_2O$ and $[UO_2L^*_2](NO_3)_2{\cdot}H_2O$[32]. The former is a 2D UOF with a tetra-nuclear uranyl oxo-cluster, and the latter is a 3D cationic UOF. In this work, by utilizing the tripodal flexible zwitterion ligand H_3LBr_3 with $UO_2(NO_3)_2{\cdot}6H_2O$ under hydrothermal conditions, we successfully synthesized a 3D cationic tetra-nuclear uranyl oxo-cluster based microporous UOF, namely, $[(UO_2)_2(\mu_3\text{-}O)(\mu_2\text{-}OH)L]NO_3{\cdot}nH_2O$ (n ≈ 5) (**1**). This UOF has been characterized by elemental analysis, IR spectroscopy, single-crystal X-ray diffraction, solid fluorescence, and powder X-ray diffraction, thermogravimetric analysis, and UV-visible spectroscopy. Furthermore, UOF **1**

showed good photocatalytic activity for the degradation of MB.

Materials and Methods

All the reagents are commercially available and were used as received, except H_3LBr_3. Elemental analyses (C, H, N) were recorded using a Vario EL III elemental analyzer. The IR spectrum was obtained using a Smart Omni-Transmission spectrometer in the range 4000–400 cm^{-1} using a KBr pellet. PXRD data were collected on a Philips X-Pert-MPD diffractometer with CuKα (λ= 1.5406 Å) radiation in the 2θ range 5–50^o. Thermogravimetric analysis was recorded on a Mettler TGA/SDTA 851 thermal analyzer in the range from room temperature to 800 °C under an N_2 flow with a heating rate of 10 °C·min^{-1}. The fluorescence spectrum of **1** was recorded using a HITACHI F-4600 spectrophotometer at room temperature. A TU-1901 UV-Vis spectrophotometer (deuterium lamp) was used to record the UV–visible is spectra for the photocatalytic degradation of MB.

Synthesis of $[(UO_2)_2(\mu_3\text{-}O)(\mu_2\text{-}OH)L]NO_3\cdot nH_2O$ (n ≈ 5) (1)

The target ligand H_3LBr_3 was synthesized in two steps according to the literature and characterized by elemental analysis[33]. A mixture of $UO_2(NO_3)_2\cdot 6H_2O$ (0.1 mmol, 50.2 mg), H_3LBr_3 (0.1 mmol, 72.3 mg), and H_2O (5 mL) was stirred to generate a clear solution. The pH of solution was carefully adjusted to 3.0 with 1 M NaOH solution. The solution was transferred to a 25 mL Teflon-lined stainless steel reactor and heated under autogenous pressure at 413 K for 72 h. After cooling to room temperature, yellow block crystals suitable for single-crystal X-ray diffraction were obtained under suction. The crystals were washed with distilled H_2O and dried in air to give **1** in 78% yield (based on H_3LBr_3). Anal. Calcd.(%) for $C_{27}H_{32}N_4O_{20}U_2$: C 26.83, H 2.67, N 4.64; found (%) for C 26.89, H 2.72, N 4.58.%. IR (cm^{-1}, KBr pellet): 3450 (s), 3380 (s), 3120 (m), 3050 (s), 2970 (w), 2820 (w), 2420 (w), 1950 (w), 1840 (w), 1640 (s), 1610 (s), 1560 (s), 1420 (s), 1380 (s), 1260 (w), 1210 (w), 1180 (w), 1130 (m), 1050 (m), 903 (s), 830 (w), 775 (s), 707 (s), 640 (w), 594 (w), 549 (w), 519 (m), 458 (m), 413 (w).

Single-crystal structure determination

The crystallographic data of **1** was collected at 150 K on a Bruker Smart Apex II CCD diffractometer with a Mo-Kα radiation source (λ = 0.71073 Å) and a graphite monochromator using the φ and ω scan modes. The data are integrated using the SAINT program[34] and solved by direct methods and refined on F^2 by full-matrix least-squares methods using the SHELXTL and Olex2 programs[35,36]. The absorption correction was carried out using the SADABS program[37]. All hydrogen atoms were refined isotropically in the riding mode using the default SHELXTL parameters, with C–H = 0.949–0.990 Å and $U_{iso}(H) = 1.2U_{eq}(C)$, while all non-hydrogen atoms were refined anisotropically. The nitrate is disordered and refined with dfix and flat commands. The about five crystal water molecules determined from TGA and EA are highly disordered, so we masked them using Olex2. The crystallographic data and structural refinements of **1** are shown in Table 1, while selected bond lengths of **1** are shown in Table 2. CCDC: 2083704 contains the supplementary

Table 1 — Crystallographic data and structure refinement summary for complex **1**

Empircal formula	$C_{27}H_{32}N_4O_{20}U_2$
M_r	1208.61
Temperature (K)	150
λ (Å)	0.71073
Crystal system, space group	Monoclinic,*C*2/*c*
a, *b*, *c*, (Å)	20.5179(9), 11.4961(5), 28.0836(14)
α, β, γ(°)	90, 107.768(1), 90
V (Å^3)	6308.3(5)
Z	8
max 2θ (°)	25.195
ρ calcd (g cm^{-3})	2.355
μ (Mo *K*α) (mm^{-1})	10.334
F(000)	4128
crystal size (mm^3)	0.25 x 0.15 x 0.10
Index ranges	$-24 \le h \le 24, -13 \le k \le 13, -33 \le l \le 33$
collected reflns	38492
unique reflns (R_{int})	5673 (0.0852)
parameters	433
GOF (F^2)	1.074
$R_1/wR_2[I > 2\sigma(I)]$	0.0401/0.0974
R_1/wR_2 (all data)	0.0588/0.1039
Residuals, *e* A^{-3}	1.631/-1.284

$^a R_1 = \sum||F_o| - |F_c||/\sum|F_o|$, $^b wR_2 = \{\sum[w(F_o^2 - F_c^2)^2]/\sum[w(F_o^2)^2]\}^{1/2}$

Table 2— Selected bond lengths (Å) in **1**

U(1)—O(3)	1.761(6)	U(1)—O(4)	1.787(6)
U(1)—O(5)	2.237(6)	U(1)—O(6)	2.281(6)
U(1)—O(7)$^{\#3}$	2.561(7)	U(1)—O(8)$^{\#3}$	2.510(7)
U(1)—O(11)	2.356(7)	U(2)—O(1)	1.762(7)
U(2)—O(2)	1.786(7)	U(2)—O(5)	2.257(6)
U(2)—O(5)$^{\#1}$	2.303(6)	U(2)—O(6)$^{\#1}$	2.448(6)

Symmetry codes: #1 3/2-x, 5/2-y, 1-z; #2 1-x, 1-y, 1-z; #3 1/2-x, 1/2+y, 1/2-z.

crystallographic data. It can be obtained free of charge from the Cambridge Crystallographic Data Centre via www.ccdc.cam.ac.uk/data_request/cif.

Results and Discussion

The crystal structure of 1

X-ray single-crystal studies showed that UOF **1** crystallizes in the monoclinic space group *C*2/*c*. As shown in Fig. 1, the skeleton unit of UOF **1** is composed of two uranyl, one zwitterion ligand (L), one μ_3-bridged oxygen atom, and one μ_2-bridged hydroxy group. Both of the U atoms are hexavalent. U1 is seven-coordinate via seven oxygen atoms: O3 and O4 from O=U=O, O7#5, O8#5, and O11 from L (#5 1/2-x, 1/2+y, 1/2-z), O5 from the μ_3-bridged oxygen atom, and O6 from the μ_2-bridged hydroxy group, with bond lengths of 1.761(6) Å to 2.561(7) Å (Table 2), forming a pentagonal bipyramid. U2 is also seven-coordinate with a pentagonal bipyramid coordination environment formed from seven oxygen atoms: O1 and O2 from O=U=O, O10#4 and O12 from L, O5 and O5#1 from the μ_3-bridged oxygen atom, and O6#1 from the μ_2-bridged hydroxy group (#1 3/2-x, 5/2-y,1-z; #4 1-x, 1-y, 1-z), with bond lengths of1.762(7) Å to 2.448(6)Å (Table 2). Two U1 and two U2 atoms are linked by O atoms to generate a tetra-nuclear oxo-cluster $[(UO_2)_4(\mu_3\text{-}O)_2(\mu_2\text{-}OH)_2(COO)_6]^{4-}$ (Fig. 1b and 1c). According to the coordination mode of L (Fig. S1, Supplementary Data), one tetra-nuclear oxo-cluster is bonded by six carboxyl groups from six molecules of L, while one L is bonded to three tetra-nuclear oxo-clusters, giving a 3D UOF structure with a 1D channel (Fig. 2). Thus, the molar ratio of uranyl *vs* L is 2:1. Because the fully deprotonated tripodal flexible zwitterion ligand is neutral, the UOF is cationic with one positive charge. The X-ray single-crystal studies show that one nitrate is trapped in the micropore to balance the charge. The IR spectrum exhibits the characteristic band due to the nitrate (1380 cm^{-1}). The water molecules located in the porous channel are

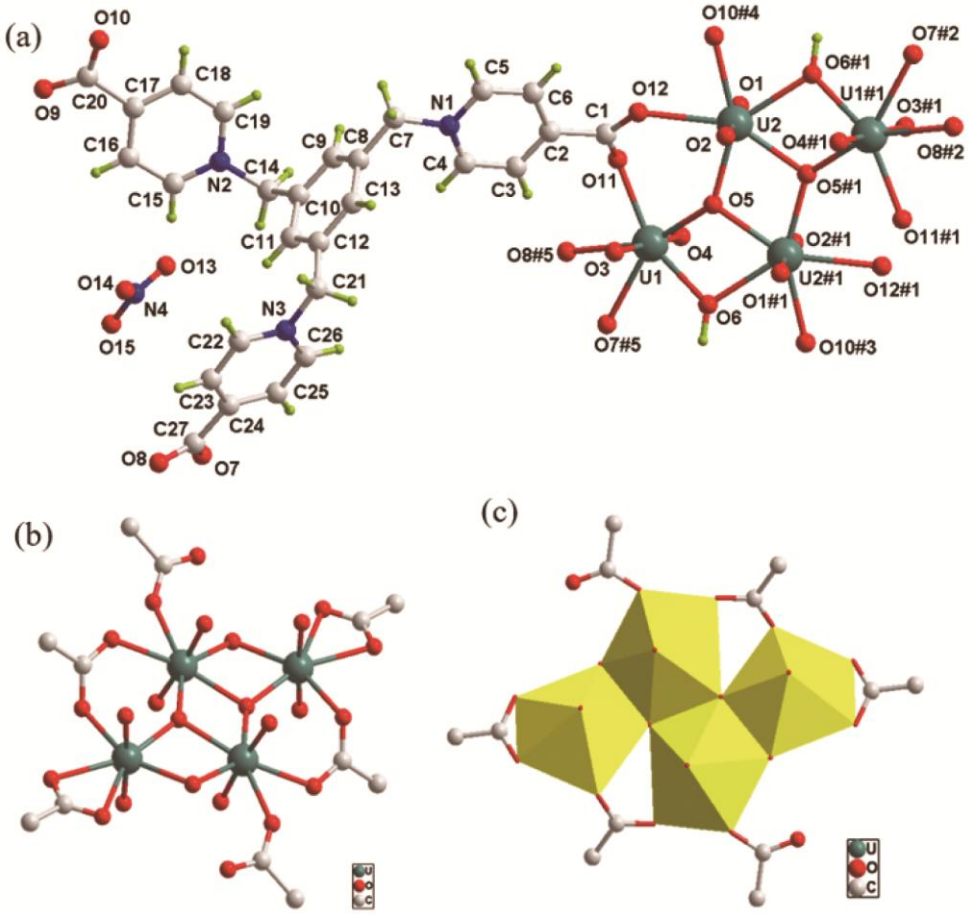

Fig. 1 — (a) Coordination environment of U(VI), (b) edge-sharing tetranuclear uranyl oxo-cluster in **1** and (c) a view of the tetranuclear uranyl polyhedron (Crystal water molecules are omitted for clarity. Symmetry codes: #1 3/2-x, 5/2-y,1-z; #2 1+x, 2-y, 1/2+z; #3 1/2+x, 3/2+y, z; #4 1-x, 1-y, 1-z; #5 1/2-x, 1/2+y, 1/2-z)

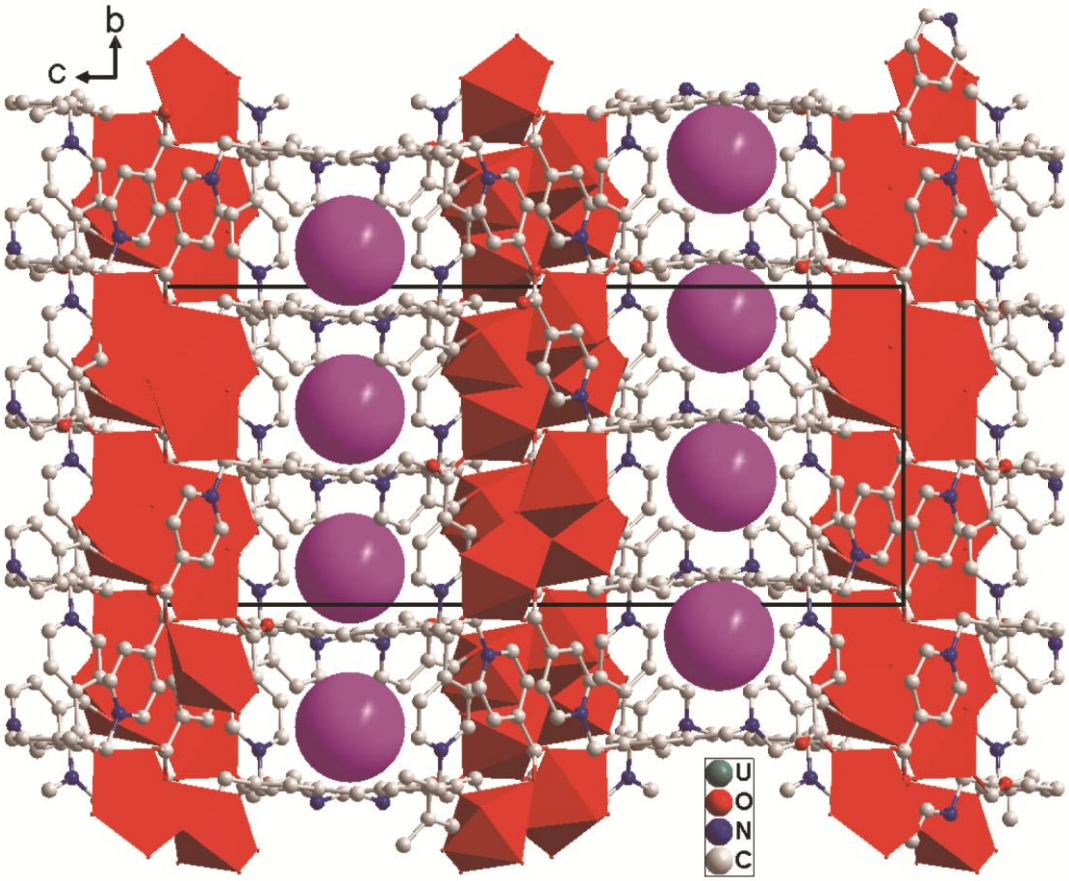

Fig. 2 — View of the 3D structure of **1**; crystal water molecules and nitrate are omitted for clarity

highly disordered and were masked by using Olex2. The number of crystal water molecules was determined from thermogravimetric analysis (TGA) and elemental analysis, giving a reasonable formula for **1**, $[(UO_2)_2(\mu_3\text{-}O)(\mu_2\text{-}OH)L]NO_3{\cdot}nH_2O$ ($n \approx 5$).

IR spectrum

Fig. S2 (Supplementary Data) shows the IR spectrum of **1**. The characteristic bands at 907 and 830 cm^{-1} are due to the stretching frequencies of the O═U═O from the uranyl group[31,32]. The peak at 1380 cm^{-1} is attributed to the characteristic band of nitrate. The peaks at 3450–3380 cm^{-1} are assigned to the O–H stretching vibrations of the crystal water molecules and coordinated hydroxy group. The stretching vibrations of O–C–O, C═N and C═C, $–CH_2–$, and Ar–H, occur at 1640 and 1610, 1560 and 1420, and 2820, and 3020 cm^{-1}, respectively.

Powder X-ray diffraction (PXRD)

The PXRD data of **1** shown in Fig. S3 (Supplementary Data) was obtained using an as-synthesized sample and was compared with the corresponding simulated single-crystal diffraction using Mercury 4.0 software. The diffraction peaks of the simulated data of **1** match perfectly with the experimental data of **1**, which confirms the phase purity of **1**.

Thermogravimetric analysis (TGA)

As shown in Fig. S4 (Supplementary Data), a two-step weight loss range from room temperature (RT) to 1073 K is observed in the TGA curve of **1**. The first-step weight loss of 7.39% (calcd 7.45%) from RT to 473 K is considered as the release of about five crystal water molecules of **1** with an obvious platform (378 K to 473 K), which indicates the good stability of the cationic UOF **1**. The second step (473 K to 823 K) is a continuous weight loss 45.12% (calcd 45.22%), which is attributed to the collapse of one hydroxy group, one nitrate, and one zwitterionic ligand. No obvious weight loss is observed after 823 K and the remaining residue is UO_3.

Fluorescence properties

The solid-state fluorescence spectrum of **1** was recorded at RT. UOF **1** displays strong green fluorescence when excited at a wavelength of 335 nm.

As shown in Fig. 3, **1** shows five typical emission peaks at 491, 513, 536, 562 and 579 nm corresponding to the electronic and vibronic transitions $S_{10}\rightarrow S_{00}$, $S_{10}\rightarrow S_{01}$, $S_{10}\rightarrow S_{02}$, $S_{10}\rightarrow S_{03}$ and $S_{10}\rightarrow S_{04}$, respectively.

UV–visible spectrum

The solid-state UV-visible spectrum of **1** at room temperature is shown in Fig. S5 (Supplementary Data). The peak at 287 nm is identified as being due to L and the peaks at 330, 410, 430, and 450 nm are assigned to uranyl, which indicates that **1** has potential photocatalytic activity in the degradation organic dyes under UV or visible light.

Photocatalytic degradation

The photocatalytic activity of **1** was evaluated using water-soluble MB as a typical model. A series of gradient concentration suspensions (0.6, 0.8, 1.0, 1.2 and 1.5 mg·mL^{-1}) were prepared by adding 30, 40, 50, 60, and 75 mg of **1** to 50 mL of 20 mg·L^{-1} MB solution, respectively. Next, they were stirred in the dark for 1 h before irradiation. The samples were continually prepared by centrifugation of the suspensions to remove the UOF material at 10 min intervals during irradiation with a LED lamp (λ > 420 nm), they were then analyzed by absorption maximum at 664 nm. As shown in Fig. 4, the MB degradation rate was 75.8%, 81.8%, 92.7%, 84.8%, and 70.6% at different concentrations of **1**. These results indicate that the highest degeneration efficiency originates from the sample with 1.0 mg·mL^{-1} of **1**.The reason may be that **1** can not give its full play to its catalytic effect in lower concentration, while **1** can't fully contact all the dyes in higher concentration, so that the excess part can't be catalyzed. The degeneration efficiency 92.7% in this work is similar to the existing uranyl complexes photocatalysts[25,30,38] and better than other previously reported results[39-41]. Fig. 5 shows the absorption spectra of MB solution during degradation with the 1.0 mg·mL^{-1} sample of **1** as the optimum catalyst dosage. From the results, we can conclude that UOF material **1** demonstrates photocatalytic activity in the degradation of MB under visible light irradiation using an LED lamp (λ> 420 nm).

At present, the mechanism of photocatalytic degradation of organic dyes by uranyl complexes is generally considered to occur in two steps: hydrogen abstraction and electron transfer [23,27,40]. U_{5f} and O_{2p} interact to each other to form HOMO ((highest occupied molecular orbitals) and LUMO (lowest unoccupied molecular orbitals) orbitals, of which O_{2p}

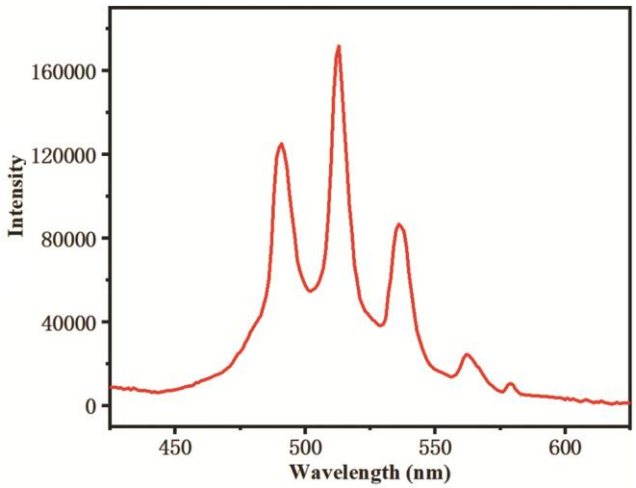

Fig. 3 — Solid-state fluorescence spectrum of **1** (λ_{ex}= 335 nm)

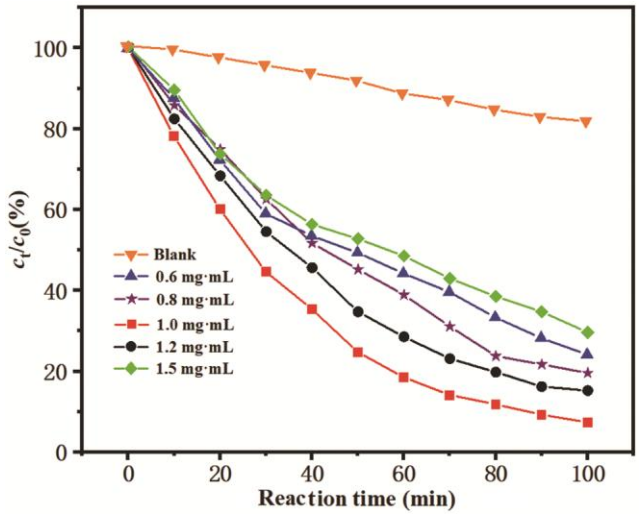

Fig. 4 — Absorption spectra for photocatalytic degradation of MB solution under UV irradiation using different concentrations of **1**

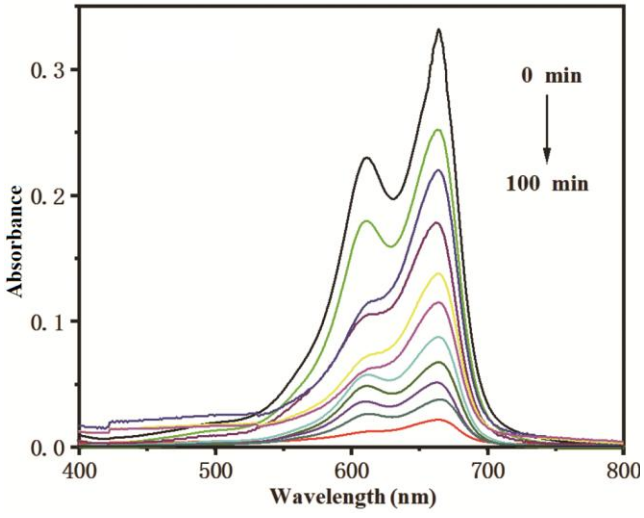

Fig. 5 — UV-visible absorption spectra of MB solution during degradation with **1** at 10 min intervals

mainly constitutes HOMO orbitals and U_{5f} mainly constitutes LUMO orbitals. Under the irradiation of an LED lamp, the electron transferred from O_{2p} to U_{5f}, that is, the charge transfer from ligand to metal, resulting that $[UO_2]^{2+}$ is excited to produce an excited state $([UO_2]^{+})^{*}$. The electron on HOMO is unstable and captured by electronegative oxygen in the solution to form highly active peroxide anions O_2^-. The LUMO orbital is easier to accept an electron from MB due to the lack of an electron, so that MB loses a proton and becomes an intermediate state, which is oxidized or degraded into small molecules by O_2 or O_2^- to complete the photocatalytic degradation process.

Conclusions

We have hydrothermally synthesized a cationic microporous 3D UOF $[(UO_2)_2(\mu_3\text{-}O)(\mu_2\text{-}OH)L]NO_3{\cdot}nH_2O$ ($n \approx 5$) (**1**) by reacting tripodal flexible zwitterionic H_3LBr_3 with uranyl nitrate hexahydrate. UOF **1** has been characterized by elemental analysis, IR spectroscopy, single-crystal X-ray diffraction, solid fluorescence and powder X-ray diffraction, thermogravimetric analysis, and absorption spectroscopy. Compound **1** exhibits strong green luminescence. In addition, we also investigated the photocatalytic activity of UOF **1** for the degradation of the organic dye MB. The results of the experiments indicate that **1** has a remarkable ability to photocatalytically degrade MB in aqueous solution, with the highest rate of degradation being 92.7% under irradiation with an LED lamp at λ> 420 nm.

Supplementary Data

Supplementary Data associated with this article are available in the electronic form at http://nopr.niscair.res.in/jinfo/ijca/IJCA_60A(11)1409-1415_SupplData.pdf.

Acknowledgment

This study was supported by the National Key Research and Development Program of China (2020YFC1909001).

References

1 Cheng L W, Liang C Y, Liu W, Wang Y X, Chen B, Zhang H L, Wang Y L, Chai Z F & Wang S A, *J Am Chem Soc*, 142 (2020) 16218.
2 Zhang M X, Liang C Y, Cheng G D, Chen J C, Wang Y M, He L W, Cheng L W, Gong S C, Zhang D, Li J, Hu S X, Diwu J, Wu G Z, Wang Y X, Chai Z F & Wang S A, *Angew Chem Int Ed*, 60 (2021) 9886.
3 Wang Y X, Yin X M, Liu W, Xie J, Chen J F, Silver M A, Sheng D P, Chen L H, Diwu J, Liu N, Chai Z F, Albrecht-Schmitt T E & Wang S A, *Angew Chem Int Ed*, 57 (2018) 7883.
4 Xie J, Wang Y X, Liu W, Yin X M, Chen L H, Zou Y M, Diwu J, Chai Z F, Albrecht-Schmitt T E, Liu G K & Wang S A, *Angew Chem Int Ed*, 56 (2017) 7500.
5 Gui D X, Duan W C, Shu J, Zhai F W, Wang N, Wang X X, Xie J, Li H, Chen L H, Diwu J, Chai Z F & Wang S A, *CCS Chem*, 1 (2019) 197.
6 Liu C, Yang X X, Niu S, Yi X Y & Pan Q J, *Dalton Trans*, 49 (2020) 4155.
7 Wu D, Mo X F, He P, Li H R, Yi X Y & Liu C, *Chem Eur J*, 27 (2021) 1.
8 Zhen T Y, Zuo L L, Yu S J,Li G H, Li G D & Chen J S, *Chem Commun*, 16 (2004) 1814.
9 Xu W, Si Z X, Xie M, Zhou L X & Zheng Y Q, *Cryst Growth Des*, 17 (2017) 2147.
10 Zhang X, Li P, Krzyaniak M, Knapp J, Wasielewski M R & Farha O K, *Inorg Chem*, 59 (2020) 16795.
11 Wang Y L, Liu Z Y, Li Y X, Bai Z L, Liu W, Wang Y X, Xu X M, Xiao C L, Sheng D P, Diwu J, Su J, Chai Z F, Albrecht-Schmitt T E & Wang S A, *J Am Chem Soc*, 137 (2015) 6144.
12 Mei L, Liu K, Wu S, Kong X H, Hu K Q, Yu J P, Nie C M, Chai Z F & Shi W Q, *Chem Eur J*, 25 (2019) 10309.
13 Liu W, Xie J, Zhang L M, Silver M A & Wang S A, *Dalton Trans*, 47 (2018) 649.
14 Wang L, Xu W, Li W Y, Xie M & Zheng Y Q, *Chem Asian J*, 14 (2019) 4246.
15 Wang L, Tu B T, Xu W, Fu Y & Zheng Y Q, *Inorg Chem*, 59 (2020) 5004.
16 Zhang N, Xing Y H & Bai F Y, *Cryst Growth Des*, 20 (2020) 1838.
17 Gao X, Wang C, Shi Z F,Jian S, Bai F Y, Wang J X & Xing Y H, *Dalton Trans*, 44 (2015) 11562.
18 Song J, Xing Y H, Wang X M, Gao X, Wang Z N, Feng X D & Bai F Y, *ChemistrySelect*, 1 (2016) 2316.
19 Wang X M, Wang C, Zhang N, Liu D Q, Wang Y & Bai F Y, *ChemistrySelect*, 5 (2020) 8625.
20 Zhang Y J, Bhadbhade M, Karatchevtseva I, Price J R, Liu H, Zhang Z M, Kong L, Cejka J, Lu K & Lumpkin G R, *J Solid State Chem*, 226 (2015) 42.
21 Reger D L, Leitner A P & Smith M D, *Cryst Growth Des*,16 (2016) 527.
22 Tian T, Yang W T, Wang H,Dang S & Sun Z M, *Inorg Chem*, 52 (2013) 8288.
23 Yu Z T, Liao Z L, Jiang Y S, Li G H & Chen J S, *Chem Eur J*, 11 (2005) 2642.
24 Li H H, Zeng X H, Wu H Y, Jie X, Zheng S T & Chen Z R, *Cryst Growth Des*, 15 (2015) 10.
25 Si Z X, Xu W & Zheng Y Q, *J Solid State Chem*, 239 (2016) 139.
26 Ren Y N, Xu W, Si Z X, Zhou L X & Zheng YQ, *Polyhedron*,152 (2018) 195.
27 Zhai X S, Zhu W G, Xu W, Huang Y J & Zheng Y Q, *CrystEngComm*, 17 (2015) 2376.
28 Hou Y N, Xing Y H, Bai F Y, Guan Q L, Wang X, Zhang R & Shi Z, *Spectrochim Acta A*, 123 (2014)267.
29 Liao Z L, Li G D, Bi M H & Chen J S, *Inorg Chem*, 47 (2008) 4844.
30 Guan Q L, Gao X, Liu J,Wei W J, Xing Y H& Bai F Y, *J Coord Chem*, 69 (2016) 1026.

31 Bai Z L, Wang Y L, Li Y X, Liu W, Chen L H, Sheng D P, Diwu J, Chai Z F, Albrecht-Schmitt T E & Wang S A, *Inorg Chem*, 55 (2016) 6358.

32 Liang L L, Zhang R L, Weng N S, Zhao J S & Liu C Y, *Inorg Chem Commun*, 64 (2016) 56.

33 Zhou J, Qiao Y F, Yan T, Wang T, Du L, Xie M & Zhao Q, *J Coord Chem*, 71 (2018) 1073.

34 SAINT, Version 8.37a, Madison, WI: Bruker AXS, 2015.

35 Sheldrick G M, SADABS, *Program for Siemens Area Detector Absorption Corrections*, University of Göttingen, Göttingen (Germany) 1997.

36 Dolomanov O V, Bourhis L J, Gildea R J, Howard J A K & Puschmann H, *J Appl Crystallogr*, 42 (2009) 339.

37 Sheldrick G M, SHELXL97, *Program for Crystal Structure Solution and Refinement*, University of Göttingen, Göttingen (Germany) 1997.

38 Ghosh S, Srivastava A K & Pal S, *New J Chem*, 43 (2019) 970.

39 Gomez G E, Onna D, D'vries R F, Barja B C, Ellena J, Narda G E & Soler-Illia G J A A, *J Mater Chem C*, 8 (2020) 11102.

40 Xu X T, Hou Y N, Wei S Y, Zhang X X, Bai F Y, Sun L X, Shi Z & Xing Y H, *CrystEngComm*, 17 (2015) 642.

41 Azam M, Velmurugan G, Wabaidur S M, Trzesowska-Kruszynska A, Kruszynski R, Al-Resayes S I, Al-Othman Z A & Venuvanalingam P, *Sci Rep*, 6 (2016) 32898.